


 Cite this: *RSC Adv.*, 2020, **10**, 11393

An effective hydroxylation route for a highly sensitive glucose sensor using APTES/GOx functionalized AlGaN/GaN high electron mobility transistor

 Jun Liu,^a Heqiu Zhang,^{ID *a} Dongyang Xue,^a Aqrab ul Ahmad,^a Xiaochuan Xia,^a Yang Liu,^a Huishi Huang,^b Wenping Guo^c and Hongwei Liang^{ID *a}

A highly sensitive glucose sensor based on AlGaN/GaN high electron mobility transistor (HEMT) has been fabricated. The hydroxyl groups on the GaN surface were achieved by the decomposition of hydrogen peroxide solution (H_2O_2) under UV irradiation for the production of hydroxyl radicals. The self-assembled monolayers (SAMs) of 3-aminopropyltriethoxysilane (APTES) with terminal amino groups formed on the hydroxylation surface were used as substrates for glucose oxidase (GOx) immobilization. The chemical groups on the GaN surface after hydroxylation were confirmed by X-ray photoelectron spectroscopy. From the analysis of current signals, the biosensor constructed with APTES/GOx exhibited good current response to glucose over a linear range from 10 to 100 μM with a sensitivity of $3.15 \times 10^4 \mu\text{A mM}^{-1} \text{cm}^{-2}$ and a detection limit of 10 nM. Meanwhile, the anticipated idea about the hydroxylation of GaN surface, can be an efficient approach for the design of AlGaN/GaN HEMT based biosensors in the future.

 Received 13th November 2019
 Accepted 5th March 2020

DOI: 10.1039/c9ra09446f

rsc.li/rsc-advances

1. Introduction

AlGaN/GaN high electron mobility transistors (HEMTs) have promising applications in high voltage and high frequency applications due to their wide band gap, high breakdown voltage, and high-mobility two dimensional electron gas (2DEG).^{1–3} Moreover, AlGaN/GaN HEMTs without doping have a high-density 2DEG near the surface,^{4,5} which is sensitive to any small changes on the surface. Therefore, AlGaN/GaN based HEMTs have recently gained more attention in the field of biosensors.^{6–11} The detection mainly works through the gating effect.¹² The conductance changes before and after the adsorption of target analytes, resulting in a potential gradient in the solution.¹³ This potential shift subsequently alters the conductance of the HEMT, leading to the change of the drain current.¹⁴

3-Aminopropyltriethoxysilane (APTES) is a material for self-assembled monolayers (SAMs), which can be combined with hydroxyl groups, aldehyde, and ethylene to realize various of applications in biosensors.^{15–17} APTES SAMs have well-controlled, ultrathin, and stable organic/inorganic interfacial characteristics.¹⁸ Moreover, APTES also has a good biocompatibility for the immobilization of biomolecules, such as glucose

oxidase (GOx).¹⁹ But it is worth to note that the hydroxylation is one of the most critical steps for the formation of APTES SAMs.²⁰ Among the most of published work, the hydroxylation method mainly used on the GaN surface is involving Piranha solution (SPM, 98% H_2SO_4 /30% H_2O_2 = 3 : 1, v/v).^{18,21} However, this hydroxylation method has strong corrosiveness, it obviously limits the flexibility of the sensor fabrication.

In this work, a highly sensitive glucose sensor based on AlGaN/GaN HEMT has been fabricated. A mild hydroxylation method on the GaN surface was developed. The APTES was covalently bonded on the hydroxylated surface through condensation reaction. The GOx can be immobilized on the APTES SAMs through electrostatic attraction. The detailed functional groups of the hydroxylated surface were analyzed using X-ray photoelectron spectroscopy (XPS). Each step of the functionalization was analyzed through *I*–*V* measurement. The proposed sensor exhibited good current response to the glucose with high sensitivity.

2. Experimental

2.1 Fabrication of AlGaN/GaN HEMT sensor

The AlGaN/GaN based HEMT epi-layers were grown on *c*-plane sapphire substrates by metal-organic chemical vapor deposition (MOCVD). The structure consisted, from bottom to top, of a 2 μm undoped GaN buffer layer, 1 nm AlN spacer, 220 \AA undoped AlGaN barrier layer with 26% Al content, and 18 \AA

^aSchool of Microelectronics, Dalian University of Technology, Dalian, P. R. China 116024. E-mail: hqzhang@dlut.edu.cn; hwliang@dlut.edu.cn

^bJiangsu Xinguanglian Technology Co., Ltd, Wuxi, Jiangsu, P. R. China 214192

^cShandong Novoshine Co., Ltd, Weifang, Shandong, P. R. China 261000



undoped GaN cap layer. The HEMT sensor fabrication process was followed by mesa isolation using inductively coupled plasma (ICP) etching with Cl_2/BCl_3 gases (100 sccm/20 sccm) under ICP power of 150 W and RF bias of 100 W at 13.6 MHz. Ti/Al/Ti/AuPt (300/2400/300/800 Å) metal stack was electron beam (e-beam) evaporated and patterned by lift-off, then annealed at 850 °C for 150 s in N_2 ambient using rapid thermal annealing (RTA). The distance between the source and drain electrodes was 80 μm . The contact resistance, calculated from the transmission line model, was $1.4 \Omega \times \text{mm}$. The sensor was then passivated with 10 000 Å SiO_2 deposited with plasma enhanced chemical vapor deposition (PECVD). 40 $\mu\text{m} \times 400 \mu\text{m}$ sensing window was opened by BOE solution ($\text{HF} : \text{NH}_4\text{F} = 1 : 6$, v/v) and had a distance of 10 μm from the source electrode. The gate electrode was separated from the active channel of the HEMT sensor and formed by e-beam evaporation, which acted as the reference electrode. Metal interconnects of Cr/Au (15/10 000 Å) were evaporated and patterned. The structure and micrograph of the fabricated HEMT sensor are shown in Fig. 1.

2.2 Hydroxylation of GaN surface

The GaN epitaxial wafer grown on c-plane sapphire substrate by MOCVD was cut into 0.25 cm \times 0.25 cm slides and cleaned ultrasonically in acetone, alcohol and deionized (DI) water for 10 min respectively, to remove the physically adsorbed contaminants, then dried by N_2 . Next, the samples were rinsed in acid solution to remove the surface metal particles and organic contaminants.²² The samples were cleaned by DI water, and dried by N_2 . After cleaning, one of the samples was immersed in 30% H_2O_2 solution under 254 nm ultraviolet (UV) light with 0.8 mW cm⁻² for 4 h, followed by 12 h incubation in H_2O_2 solution. The distance between the UV lamp and the sample was maintained at 8 cm during UV irradiation. In addition, one of the samples was immersed in 30% H_2O_2 solution for 16 h without UV irradiation. Then, all samples were cleaned ultrasonically in DI water, and dried by N_2 . The chemical groups on the GaN surface were measured by XPS (ESCALAB 250XI). XPS spectra were obtained by using monochromatic aluminum (Al) K_α X-ray ($\hbar\nu = 1486.6$ eV). The angle between the incident X-ray beam and the surface of sample was kept at 32°. All binding energies were referenced to the adventitious carbon C 1s peak position at 284.6 eV. The hydrophilic nature of the samples was characterized by measuring the contact angle with

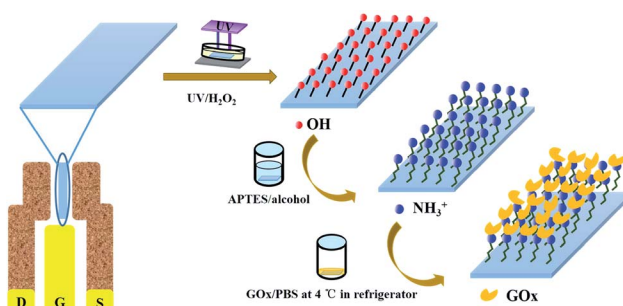


Fig. 2 Schematic illustration of the functionalization process on the AlGaN/GaN HEMT sensor.

2 μl water droplet at room temperature (WCA, POWERREACH, and JC2000C1).

2.3 APTES/GOx functionalization on the fabricated sensor

For the formation of APTES on the sensing surface, the above hydroxylation method was utilized on the AlGaN/GaN HEMT based sensor. Then, the hydroxylated HEMT sensor was placed inside the APTES/ethanol mixture solution (2%, v/v), covered with the preservative film, and incubated in dark room for 24 h. After incubation, the sensor was cleaned ultrasonically in ethanol and DI water to remove the residual APTES. After that, 10 mg mL⁻¹ GOx solution in 0.01 M phosphate buffer solution (1×, PBS) was dropped on the sensor and incubated at 4 °C for 48 h. The incubated sensor was washed in DI water to remove the residual GOx. The sensor was incubated at 37 °C for 30 min to activate the GOx. The prepared sensor was stored at 4 °C until further usage. The schematic diagram about the functionalization processes is shown in Fig. 2.

Glucose oxidase type X-S (GOx, 135 200 units per g, EC1.1.3.4. From aspergillus Niger), APTES solution (99%) and glucose powder were purchased from Sigma Aldrich. PBS solution (Na_2HPO_4 8 mM, NaCl 136 mM, KH_2PO_4 2 mM, KCl 2.6 mM) was purchased from solarbio (China). The aqueous glucose solution was prepared 24 h prior to measurements, in order to obtain its biologically active form (β -D-glucose).²³

3 Results and discussion

3.1 XPS analysis

For the investigation of chemical groups on the hydroxylated GaN surface by XPS analysis, three types of samples were prepared: without treated (untreated), with H_2O_2 treated and UV-irradiating H_2O_2 solution (UV/ H_2O_2) treated samples, respectively. Fig. 3(a) shows the core-level C 1s XPS spectra of all three samples. The core-level C 1s peak is further divided into four peaks ascribed to C=C (284.6 eV), C-OH (285.3 eV), C=O (286.5 eV), and C (O)-O (288.6 eV). From the calculation of C 1s peak area in Fig. 3(b), it can be observed that there has no observable change in peak area of C-OH. However, the increases in peak area ratio of C=C for H_2O_2 treated and UV/ H_2O_2 treated GaN surface were observed relative to the untreated surface. This may be due to the surface easier to

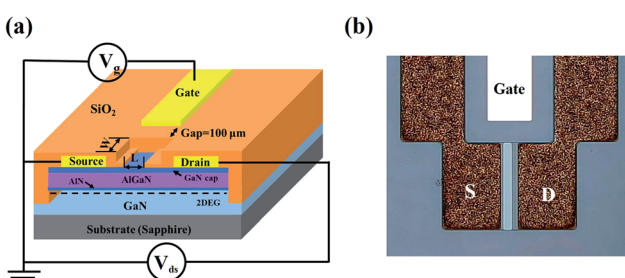


Fig. 1 (a) Schematic structure of AlGaN/GaN HEMT sensor, (b) micrograph of the fabricated HEMT sensor.



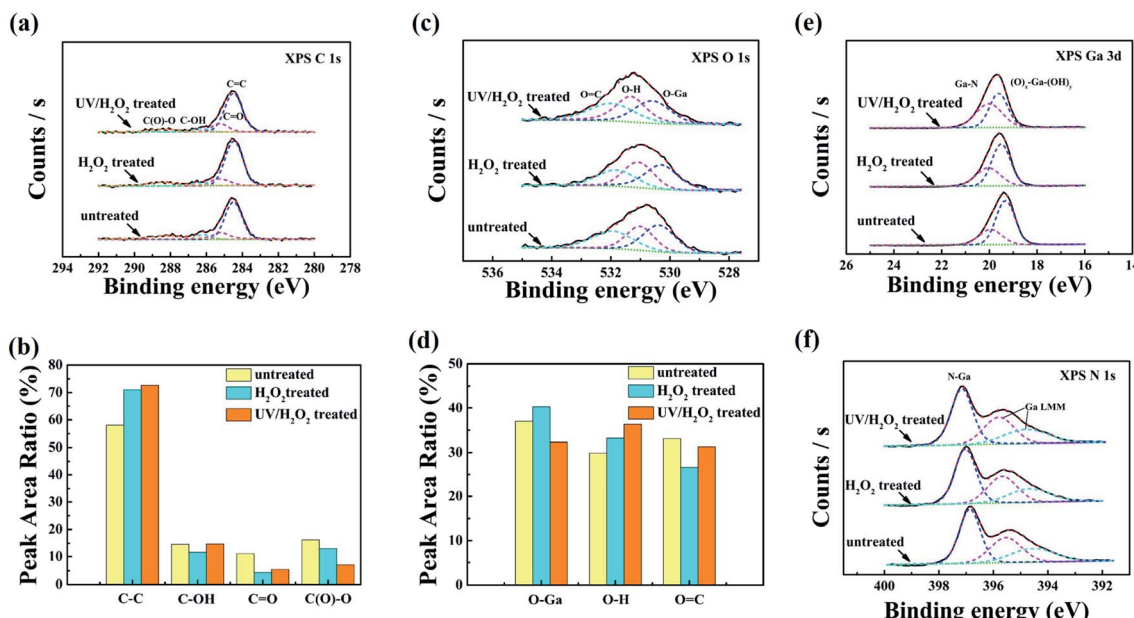


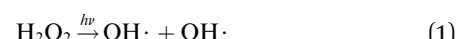
Fig. 3 The hydroxylated GaN (0001) surface with different treatments. (a) the XPS spectra of C 1s core-level. (b) The calculated peak area ratio of C 1s. (c) The XPS spectra of O 1s core-level. (d) The calculated peak area ratio of O 1s. (e) and (f) The XPS spectra of Ga 3d and N 1s core-level, respectively.

adsorb air pollutants from the low energy containments, leading to an increased C=C ratio. As shown in Fig. 3(c), the broader peak of O 1s can be divided into three peaks corresponding to O-Ga (530.4 ± 0.2 eV), O-H (531.0 ± 0.2 eV), O=C (531.8 ± 0.2 eV), respectively. Fig. 3(d) describes the correlation among the peak area ratio of O-Ga, O-H and O=C determined from the O 1s peaks. It can be observed that the peak area ratio of O-Ga after H₂O₂ treated was higher than the untreated and UV/H₂O₂ treated samples. Our Results are consistent with previously reported literature about the formation of thin GaO_x layer on the GaN surface after immersing in H₂O₂ solution at room temperature.²⁴ The peak area ratio of O=C was reduced after H₂O₂ or UV/H₂O₂ treated. Removal of the adsorbed carbonaceous material from the GaN surface resulted in a decreased O=C ratio. However, the peak area ratio of O-H on the GaN surface after UV/H₂O₂ treatment was significantly higher than the other samples. These results indicated that the hydroxyl groups can be achieved on the GaN surface after UV/H₂O₂ treatment.

In Fig. 3(e), Ga 3d spectra are divided into two components with an increasing order of chemical shifts, corresponding to Ga-N, O_x-Ga-(OH)_y. Moreover, herein O_x-Ga-(OH)_y indicates a mixed phase consisting of Ga-O_x and Ga-(OH)_y. Comparing with the untreated sample, the peak area ratio of O_x-Ga-(OH)_y increased from 29.3% to 49.6% after UV/H₂O₂ treatment. Due to the formation of metal oxides on the surface,⁸ the peak area ratio of O_x-Ga-(OH)_y also slightly increased from 29.3% to 35.7% after H₂O₂ treatment. In Fig. 3(f), N 1s spectra consist of N-Ga (397 ± 0.2 eV), and two Ga LMM Auger electrons with satellites from lower energy side.^{25,26} There is no change observed in N 1s spectra of all three samples. Combining with O 1s analysis, it can be concluded that the hydroxyl groups

combined with Ga-sites can be obtained on the GaN surface after UV/H₂O₂ treatment.

The mechanism of surface hydroxylation is based on the photo-assisted reactions, which takes oxygen as the only electron acceptor.²⁷ Under UV irradiation, the photogeneration of hydroxyl radicals (OH[·]) are the main oxidants formed in the decomposition of H₂O₂ solution. It is extremely reactive with Ga-sites.²⁸ This is consistent with the analysis results of the hydroxylated GaN surface by XPS. The photo-assisted process is illustrated by the following eqn (1):²⁹



In current experiment, the average WCAs of the untreated and H₂O₂ treated GaN surface were 26° and 11° , respectively. However, the average WCA on the GaN surface after UV/H₂O₂ treatment was less than 5° . These results indicated that the UV/H₂O₂ treatment can enhance the surface hydrophilicity more effectively, which is beneficial for the hydroxylation of the surface.

3.2 Electrical measurement and analysis of the fabricated sensor

Fig. 4(a) shows the *I*-*V* characteristics of each step functionalization on the HEMT sensor without gate bias voltage. It can be observed that there is a significant difference in the source-drain saturation current after each step functionalization. Comparing with the non-functionalized (bare) sensor, the drain current was decreased after the sensing surface hydroxylation. However, the drain current was increased after the APTES formed on the hydroxylated sensing surface. Then, the

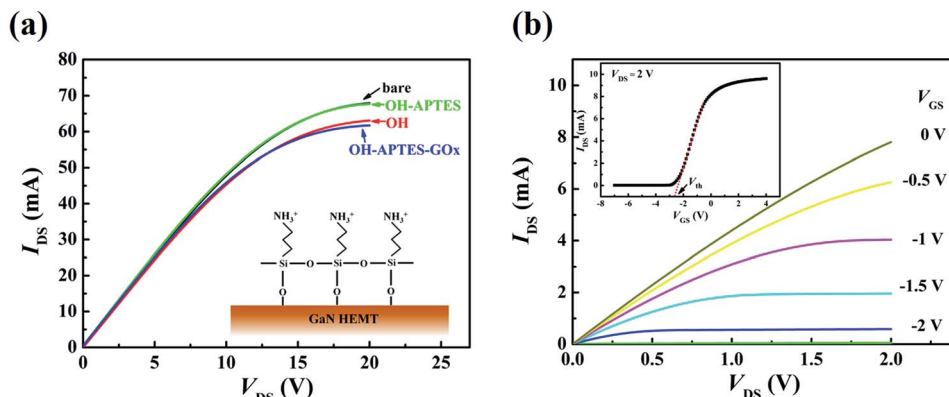


Fig. 4 (a) The electrical characteristics of each step functionalization on HEMT sensor without bias voltage on the gate. (b) Output characteristics of the prepared sensor upon 1× PBS solution for several gate voltages swept from -4 V to 0 V in steps of 0.5 V, the inset shows the transfer characteristic at $V_{DS} = 2$ V.

immobilization of GOx made the current value decrease. The measurement mechanism is based on the change of negative or positive charges on the sensing surface, which will reduce or increase the carrier concentration of 2DEG at the AlGaN and GaN interface. The process of hydroxylation reduced the positive charge on the surface after the hydroxyl groups combined with GaN surface, leading a decreased drain current signal. In contrast, when the APTES covalently bonded on the

hydroxylated surface though the dehydration-condensation reaction, the amino-terminated groups ($-\text{NH}_2$) of APTES were easily changed to the positively charged ions ($-\text{NH}_3^+$) by adsorption the hydrogen ion (H^+) in aqueous solution.³⁰ Therefore, the drain current increased after APTES immobilized on the hydroxylated surface. Meanwhile, the construction of APTES on the hydroxylation surface can be deduced from I - V characteristics (Fig. 4(a) inset at the bottom right). By

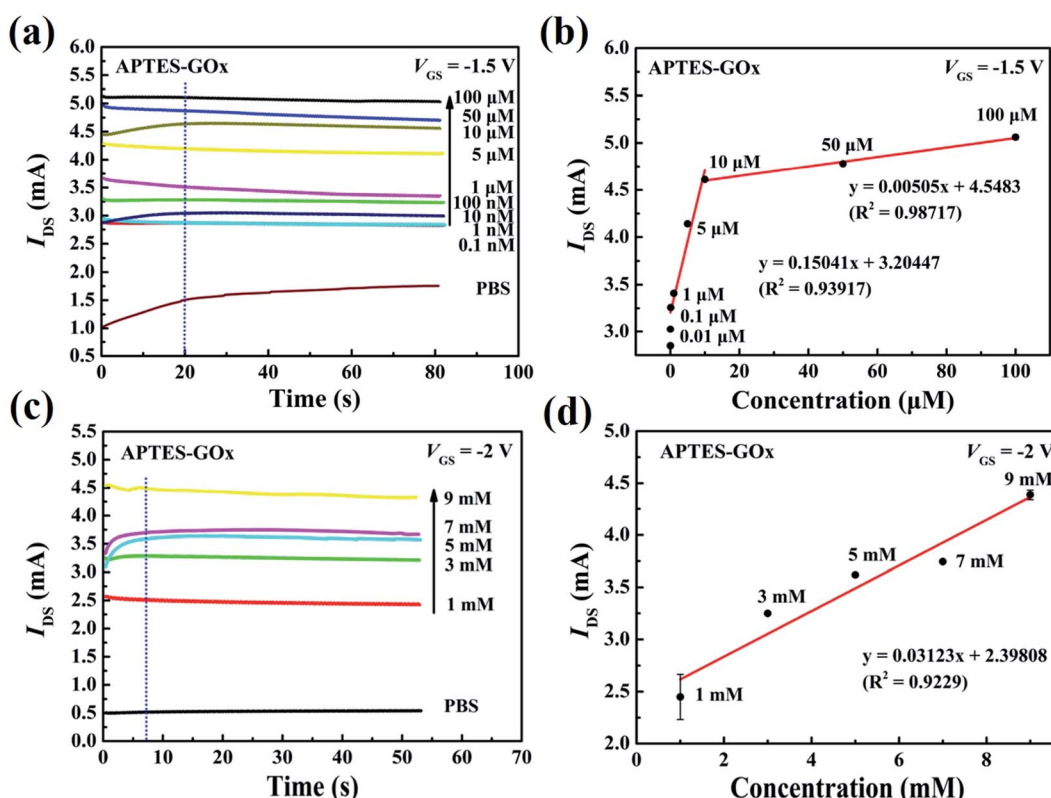


Fig. 5 (a) Current versus time graph with APTES-GOx functionalized on the open-gated surface in the presence of different glucose concentrations, and (b) current versus different concentration of glucose between 0.01 and 100 μM at a gate potential of -1.5 V. (c) Current versus time graph with APTES-GOx functionalized on the open-gated surface in the presence of different glucose concentrations, and (d) current versus different concentration of glucose solutions between 1 mM and 9 mM at a gate potential of -2 V.



comparing the drain current variation (ΔI) of each step functionalization, it can be inferred that the three ethyl groups of APTES can all react with the hydroxyl groups on the sensing surface, which contributes to the formation of the APETS SAMs with good orientation.¹⁸ The construction of APTES was also confirmed that the UV/H₂O₂ treatment can produce enough hydroxyl groups on the sensing surface. Furthermore, from the results of the following glucose detection, it is clear that GOx molecules were present on the sensing region.

The output characteristics upon 1× PBS solution are shown in Fig. 4(b), and the inset displays the transfer characteristic. The detection mainly works through the gating effect. The equivalent circuit of gate can be simplified as series two-plate capacitance. Due to the capacitances are in series, the equivalent capacitance and electrical impedance are defined as (2) and (3):¹³

$$\frac{1}{C} = \frac{1}{C_s} + \frac{1}{C_{\text{FET}}} \quad (2)$$

$$Z_c = \frac{1}{j\omega C} \quad (3)$$

where C_s and C_{FET} are the solution capacitance and transistor capacitance, j and ω represent the phase information, respectively. The solution capacitance C_s changes before and after the adsorption of target analytes in the solution. Then the net potential drop creates a potential gradient in the solution. This potential shift on the gate region subsequently modulates the drain current. These are expected to obey the following eqn (4)–(6):^{31,32}

$$V_{\text{GS}} = \Delta V_s + \Delta V_{\text{FET}} \quad (4)$$

$$\Delta V_{\text{FET}} = \frac{\frac{1}{j\omega C_{\text{FET}}}}{\frac{1}{j\omega C_s} + \frac{1}{j\omega C_{\text{FET}}}} \times V_{\text{GS}} = \frac{C_s}{C_{\text{FET}} + C_s} \times V_{\text{GS}} \quad (5)$$

$$I_{\text{DS}} = \frac{\mu W C_{\text{FET}}}{L} \left[(V_{\text{GS}} - V_{\text{th}}) V_{\text{DS}} - \frac{V_{\text{DS}}^2}{2} \right] \quad (6)$$

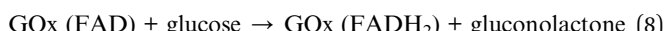
where ΔV_s and ΔV_{FET} are the gate voltage drops in solution and in transistor, V_{th} is the threshold voltage, μ is the mobility of 2DEG, W is the width of the gate, L is the length of the gate. When $V_{\text{DS}} \geq V_{\text{GS}} - V_{\text{th}} = V_{\text{DS sat}}$, eqn (6) is given by:

$$I_{\text{DS sat}} = q W v_{\text{sat}} n_s = \frac{\mu W C_{\text{FET}}}{L} \times \frac{1}{2} (V_{\text{GS}} - V_{\text{th}})^2 \quad (7)$$

where $I_{\text{DS sat}}$ is the saturation current, q is the electronic charge, v_{sat} is the saturation velocity, n_s is the 2DEG concentration. Clearly source-drain saturation current is proportional to the square of the gate voltage. Therefore, a negative gate voltage of 1.5 V and 2 V was applied, which can provide a higher amplified output signal for glucose detection.

3.3 The performance of the fabricated sensor for glucose detection

Fig. 5 shows the current response curves of APTES/GOx functionalized sensor for the additions of glucose. As shown in Fig. 5(a), the value of the drain current increased from 3.24 mA to 5.04 mA at a gate potential of -1.5 V, corresponding to the glucose concentration ranging from 0.1 μM to 100 μM . And the response time was approximately 20 s. Fig. 5(b) shows the calibration curves at $V_{\text{GS}} = -1.5$ V, which was obtained from the sensor with APTES/GOx functionalization. The current response increased linearly with glucose concentrations from 0.1 to 10 μM and from 10 to 100 μM . The sensitivity obtained was of 9.4×10^5 and $3.15 \times 10^4 \mu\text{A mM}^{-1} \text{cm}^{-2}$, respectively. Fig. 5(c) shows the current response to glucose at a gate potential of -2 V. The current response gradually increased with the increase of glucose and reached a steady-state current value within 10 s. The linear calibration range was extended up to 9.0 mM with a sensitivity of $1.95 \times 10^5 \mu\text{A mM}^{-1} \text{cm}^{-2}$ in Fig. 5(d). These results revealed that the sensor exhibited electrocatalytic activity towards glucose that is expressed as follows:



where GOx (FADH₂) and GOx (FAD) represent reduced and oxidized forms of GOx. According to reaction (8) and (9), the oxidized form of GOx is reduced to GOx (FADH₂). Then the formed GOx (FADH₂) returns to its native oxidized form and releases two protons (2H⁺) and two electrons (2 e⁻). The different concentration of glucose can release different numbers of protons and electrons, inducing the change of the solution capacitance. The changed solution capacitance can

Table 1 Comparison of the APTES/GOx functionalized AlGaN/GaN HEMT biosensor with other glucose biosensors previously reported

Biosensor	Linear range	Sensitivity ($\mu\text{A mM}^{-1} \text{cm}^{-2}$)	Reference
Nafion/GOx/ZnO nanorods/ITO	0.05–1.00 mM 1.00–20.00 mM	48.75 3.87	33
Nf/PdNPs/rGO-APTES/GOx/GCE	3 μM to 4.57 mM	234.1	19
PET/QCS-MOx-OD/GOx electrode	1–111 mM	176	34
CoWO ₄ /CNT/CNT-AuNS	0–0.3 mM	10.89	35
CQDs-AuNPs-GOx	0.16–4.32 mM	626.06	36
APTES/GOx/AlGaN/GaN HEMT	0.1–10 μM 10 μM to 100 μM 1–9 mM	9.4×10^5 3.15×10^4 1.95×10^5	This work



modulate the drain current of the channel from eqn (2)–(7). Such extended linear range should attribute to the GOx immobilization and the gate voltage applied to the sensor. APTES SAMs provide a suitable environment to retain the GOx activity. And testing in saturation region can get a highly amplified signal of the product of the enzymatic reaction. The comparison of the performance of the fabricated biosensor with other glucose biosensor was presented in Table 1.

The current response to glucose was measured after the 30th day since the APTES/GOx functionalized sensor was prepared. The presented biosensor exhibited a high sensitivity to glucose even after a month. However, the saturated drain current upon 1× PBS solution decreased 26% and 28%, corresponding to the gate voltage of -2 V and -1.5 V , respectively. The change of the output characteristics should be related to the surface state of the sensing region. Cleaning and storage of the sensor might be the main reason for the drain current drop.

4. Conclusions

In this work, a mild hydroxylation process for GaN surface to develop highly sensitive APTES/GOx functionalized HEMT glucose biosensor was presented. The fabricated biosensor exhibited good current response to glucose with linear range from 0.1 to $10\text{ }\mu\text{M}$ and from 10 to $100\text{ }\mu\text{M}$ at a gate voltage of -1.5 V , and had high sensitivity of 9.4×10^5 and $3.15 \times 10^4\text{ }\mu\text{A }\text{mM}^{-1}\text{ cm}^{-2}$, respectively. Moreover, the presented biosensor showed a linear range from 1 mM to 9 mM with a sensitivity of $1.95 \times 10^5\text{ }\mu\text{A }\text{mM}^{-1}\text{ cm}^{-2}$ at a gate voltage of -2 V . Hence, the assembled APTES/GOx on the hydroxylation surface exhibited an electrocatalytic activity to glucose. The low gate voltage enhanced the measurement signal. The APTES/GOx functionalized AlGaN/GaN HEMT can be utilized to real application after optimization in future work.

Conflicts of interest

There are no conflicts to declare.

Acknowledgements

This work was supported by National Science Foundation of China (No. 61574026, 11675198), National Key R&D Plan (No. 2016YFB0400600, 2016YFB0400601), Liaoning Provincial Natural Science Foundation of China (No. 201602176), the Major Projects of Science and Technology in Shandong Province (No. 2015ZDJQ03003).

References

- 1 A. Link, T. Graf, R. Dimitrov, O. Ambacher, M. Stutzmann, Y. Smorchkova, U. Mishra and J. Speck, *Phys. Status Solidi B*, 2001, **228**, 603–606.
- 2 T. S. Narihiko Maeda, K. Tsubaki, T. Nishida and N. Kobayashi, *Appl. Phys. Lett.*, 2000, **76**, 3118–3120.
- 3 Y. S. C. Sourabh Khandelwal and T. A. Fjeldly, *IEEE Trans. Electron Devices*, 2012, **59**, 2856–2860.
- 4 O. Ambacher, B. Foutz, J. Smart, J. R. Shealy, N. G. Weimann, K. Chu, M. Murphy, A. J. Sierakowski, W. J. Schaff, L. F. Eastman, R. Dimitrov, A. Mitchell and M. Stutzmann, *J. Appl. Phys.*, 2000, **87**, 334–344.
- 5 H. W. Jang, C. M. Jeon, K. H. Kim, J. K. Kim, S.-B. Bae, J.-H. Lee, J. W. Choi and J.-L. Lee, *Appl. Phys. Lett.*, 2002, **81**, 1249–1251.
- 6 M. L. S. Xuejin Wen, S. K. Gupta, T. R. Nicholson III, S. C. Lee and W. Lu, *IEEE Sens. J.*, 2011, **11**, 1726–1735.
- 7 G. Steinhoff, B. Baur, H.-G. von Ribbeck, G. Wrobel, S. Ingebrandt, A. Offenhäusser, M. Stutzmann and M. Eickhoff, *Adv. Solid State Phys.*, 2005, **45**, 363–374.
- 8 O. P. G. Steinhoff, M. Tanaka, M. Stutzmann and M. Eickhoff, *Adv. Funct. Mater.*, 2003, **13**, 841–846.
- 9 C. Warnke, H. Witte, T. Mair, M. J. B. Hauser, A. Dadgar and A. Krost, *Sens. Actuators, B*, 2010, **149**, 310–313.
- 10 N. Espinosa, S. U. Schwarz, V. Cimalla, A. Podolska and O. Ambacher, *Procedia Eng.*, 2015, **120**, 912–915.
- 11 B. S. Kang, H. T. Wang, F. Ren, S. J. Pearton, T. E. Morey, D. M. Dennis, J. W. Johnson, P. Rajagopal, J. C. Roberts, E. L. Piner and K. J. Linthicum, *Appl. Phys. Lett.*, 2007, **91**, 252103.
- 12 S. Mao, J. Chang, H. Pu, G. Lu, Q. He, H. Zhang and J. Chen, *Chem. Soc. Rev.*, 2017, **46**, 6872–6904.
- 13 C.-H. Chu, I. Sarangadharan, A. Regmi, Y.-W. Chen, C.-P. Hsu, W.-H. Chang, G.-Y. Lee, J.-I. Chyi, C.-C. Chen, S.-C. Shiesh, G.-B. Lee and Y.-L. Wang, *Sci. Rep.*, 2017, **7**, 5256.
- 14 M. Kaisti, *Biosens. Bioelectron.*, 2017, **98**, 437–448.
- 15 P. Yang and W. Yang, *ACS Appl. Mater. Interfaces*, 2014, **6**, 3759–3770.
- 16 L. S. Jang and H. J. Liu, *Biomed. Microdevices*, 2009, **11**, 331–338.
- 17 G. A. Castillo, L. Wilson, K. Efimenko, M. D. Dickey, C. B. Gorman and J. Genzer, *ACS Appl. Mater. Interfaces*, 2016, **8**, 35641–35649.
- 18 C. P. A. Arranz, D. García-Fresnadillo, G. Orellana, A. Navarro and E. Muoz, *Langmuir*, 2008, **24**, 8667–8671.
- 19 M. Guler and Y. Dilmac, *J. Electroanal. Chem.*, 2019, **834**, 49–55.
- 20 A. Ulman, *Chem. Rev.*, 1996, **96**, 1533–1554.
- 21 B. Baur, G. Steinhoff, J. Hernando, O. Purrucker, M. Tanaka, B. Nickel, M. Stutzmann and M. Eickhoff, *Appl. Phys. Lett.*, 2005, **87**, 263901.
- 22 F. Machuca, Z. Liu, Y. Sun, P. Pianetta, W. E. Spicer and R. F. W. Pease, *J. Vac. Sci. Technol. A*, 2002, **20**, 1784–1786.
- 23 M. David, M. M. Barsan, C. M. A. Brett and M. Florescu, *Sens. Actuators, B*, 2018, **255**, 3227–3234.
- 24 H.-I. C. Chun-Chia Chen, I.-P. Liu, H.-Y. Liu, P.-C. Chou, J.-K. Liou and W.-C. Liu, *Sens. Actuators, B*, 2015, **211**, 303–309.
- 25 A. N. Hattori, K. Endo, K. Hattori and H. Daimon, *Appl. Surf. Sci.*, 2010, **256**, 4745–4756.
- 26 A. N. Hattori, F. Kawamura, M. Yoshimura, Y. Kitaoka, Y. Mori, K. Hattori, H. Daimon and K. Endo, *Surf. Sci.*, 2010, **604**, 1247–1253.
- 27 J. Zuo and E. Torres, *Langmuir*, 2010, **26**, 15161–15168.



28 N. Chaniotakis and N. Sofikiti, *Anal. Chim. Acta*, 2008, **615**, 1–9.

29 L. F. Keyser, *J. Phys. Chem.*, 1980, **84**, 1659–1663.

30 Y. Zhang, Y. Li, W. Wu, Y. Jiang and B. Hu, *Biosens. Bioelectron.*, 2014, **60**, 271–276.

31 I. Sarangadharan, A. Regmi, Y. W. Chen, C. P. Hsu, P. C. Chen, W. H. Chang, G. Y. Lee, J. I. Chyi, S. C. Shiesh, G. B. Lee and Y. L. Wang, *Biosens. Bioelectron.*, 2018, **100**, 282–289.

32 X. Jia, D. Chen, L. Bin, H. Lu, R. Zhang and Y. Zheng, *Sci. Rep.*, 2016, **6**, 27728.

33 N. S. Ridhuan, K. Abdul Razak and Z. Lockman, *Sci. Rep.*, 2018, **8**, 13722.

34 Z. Liang, J. Zhang, C. Wu, X. Hu, Y. Lu, G. Wang, F. Yu, X. Zhang and Y. Wang, *Biosens. Bioelectron.*, 2020, **155**, 112105.

35 S. Y. Oh, S. Y. Hong, Y. R. Jeong, J. Yun, H. Park, S. W. Jin, G. Lee, J. H. Oh, H. Lee, S. S. Lee and J. S. Ha, *ACS Appl. Mater. Interfaces*, 2018, **10**, 13729–13740.

36 V. Buk and M. E. Pemble, *Electrochim. Acta*, 2019, **298**, 97–105.

